

Peculiarities of superconducting properties of thin superconductor-normal metal bilayer with large ratio of resistivities

D. Yu. Vodolazov*

*Institute for Physics of Microstructures, Russian Academy of Sciences,
603950, Nizhny Novgorod, GSP-105, Russia and
Physics Department, Moscow State University of Education, Moscow, Russia*

E. E. Pestov, S. N. Vdovichev, S. S. Ustavshikov, and A. Yu. Aladyshkin

*Institute for Physics of Microstructures, Russian Academy of Sciences,
603950, Nizhny Novgorod, GSP-105, Russia and
Lobachevsky State University of Nizhny Novgorod,
23 Gagarin Avenue, 603950 Nizhny Novgorod, Russia*

M. Yu. Levichev, A. V. Putilov, P.A. Yunin, A. I. El'kina, N. N. Bukharov, and A. M. Klushin
Institute for Physics of Microstructures, Russian Academy of Sciences, 603950, Nizhny Novgorod, GSP-105, Russia

(Dated: November 12, 2021)

We demonstrate, both theoretically and experimentally, that thin dirty superconductor-normal metal bilayer with resistivity of normal metal ρ_N much smaller than normal-state resistivity of superconductor ρ_S has unique superconducting properties. First of all the normal layer provides the dominant contribution to the diamagnetic response of whole bilayer structure in wide temperature interval below the critical temperature due to proximity induced superconductivity. Secondly, the presence of the normal layer may increase the critical current I_c in several times (the effect is not connected with enhanced vortex pinning), provides strong temperature dependence of both I_c and effective magnetic field penetration depth even at temperatures much below the critical one and leads to the diode effect in parallel magnetic field. Besides of general interest we believe that the found results may be useful in construction of different kinds of superconducting detectors.

PACS numbers:

I. INTRODUCTION

If superconductor (S) is attached to the normal metal (N) and the SN interface is transparent for electron motion then superconducting electrons penetrate the normal metal on the characteristic length scale $\xi_N(T)$. It leads to superconducting properties of the normal metal, namely, it can carry non-dissipative current and screen applied magnetic field. The screening effect was observed experimentally in many works on different SN systems [1–3] at temperatures much below the critical temperature of the superconductor T_{c0} and the theory of this effect was developed both in clean and dirty limits using Eilenberger or Usadel equations [4–8].

Here we demonstrate that thin low resistive normal (N) layer placed on the superconducting (S) layer with large normal-state resistivity ρ_S can considerably increase its superconducting properties, namely considerably enhances the diamagnetic response and critical current I_c . We argue that the effect comes from proximity induced superconductivity and locally smaller London penetration depth λ in N-layer - see inset in Fig. 1(a). In this system the critical current enhancement is not con-

nected with enhanced vortex pinning in SN bilayer but it is related with large superconducting current density $j_s \sim 1/\lambda^2$ in N-layer. The strong temperature dependence of I_c even at $T \ll T_c$, suppression of I_c in rather weak perpendicular magnetic field, the diode effect in parallel magnetic field and enhanced diamagnetism validates in favor of this interpretation of the found experimental results.

We have to mention that the critical current density j_{cN} in N-layer of dirty SNS trilayer with thickness of N-layer $d_N \ll \xi_N(T) = (\hbar D_N/k_B T)^{1/2}$, thickness of S-layer $d_S \gg \xi_c = (\hbar D_S/k_B T_{c0})^{1/2} \sim \xi(0)$ ($D_{S(N)}$ is a diffusion coefficient of corresponding layers, T_{c0} is the critical temperature of superconductor, $\xi(0)$ is the zero temperature superconducting coherence length) and ratio of resistivities $\rho_S/\rho_N \gg 1$ first was analytically calculated in Refs. [9, 10]. Authors predicted that j_{cN} may exceed depairing current density j_{dep} of the superconductor and $j_{cN}(T) \sim 1/\sqrt{T}$ but they did not calculate the critical current of whole structure. Our calculations show that N-layer could lead to enhancement of critical current I_c of whole bilayer and nontrivial $I_c(T)$ only at low temperatures $T \ll T_{c0}$ when thickness of S or N layers exceed several ξ_c (for bilayer with realistic $\rho_S/\rho_N \lesssim 200$) while in wide temperature interval nontrivial $I_c(T)$ exists when $d_S, d_N \lesssim 2\xi_c$. Because in Refs. [9, 10] the symmetric SNS system was studied the diode effect in parallel magnetic

*Electronic address: vodolazov@ipmras.ru

field was absent.

The structure of the paper is following. In Sec. II we present our theoretical results. In Sec. III we show results of the experiment and in Sec. IV we compare our experimental and theoretical results, discuss their relation with other experiments and possible application of such bilayers.

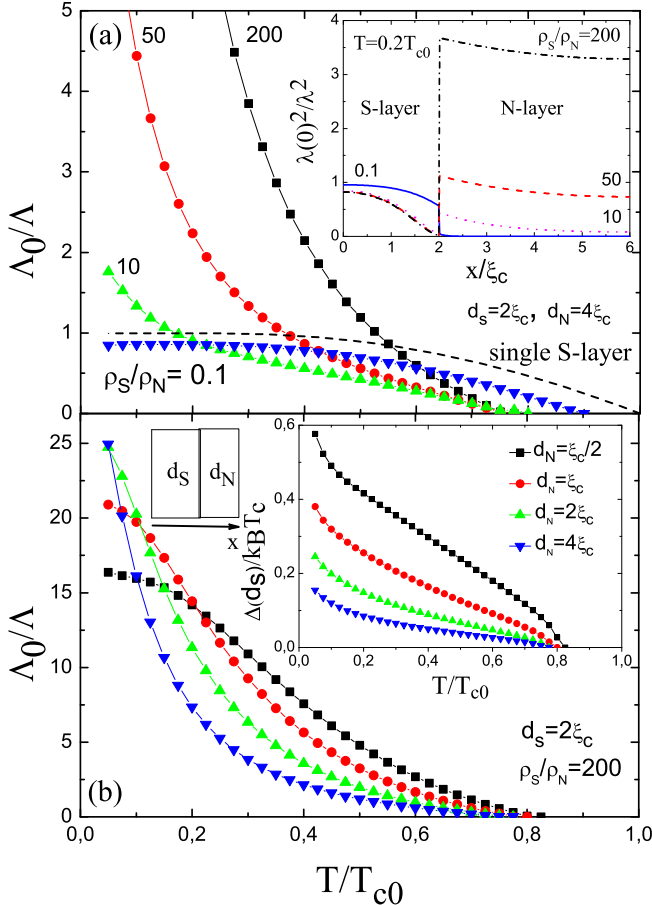


FIG. 1: Temperature dependence of inverse effective magnetic field penetration depth Λ^{-1} of SN bilayer at different $\rho_S/\rho_N = 200, 50, 10, 0.1$ (a) and different thicknesses of N-layer $d_N/\xi_c = 1/2, 1, 2, 4$ (b). In inset to Fig. 1(a) we show dependence of local $1/\lambda^2$ across the thickness of bilayer. In S-layer $1/\lambda^2$ is strongly suppressed near SN interface due to inverse proximity effect. In inset to Fig.1(b) we present dependence $\Delta(d_S)(T)$ (Δ near SN interface) to demonstrate its correlation with $\Lambda^{-1}(T)$.

II. THEORETICAL RESULTS

To calculate superconducting properties of SN bilayer we mainly use Usadel equation for anomalous F and normal G Green functions (equations and details of numerical calculations are present in Appendix A). In Fig. 1(a,b) we show calculated inverse effective magnetic field

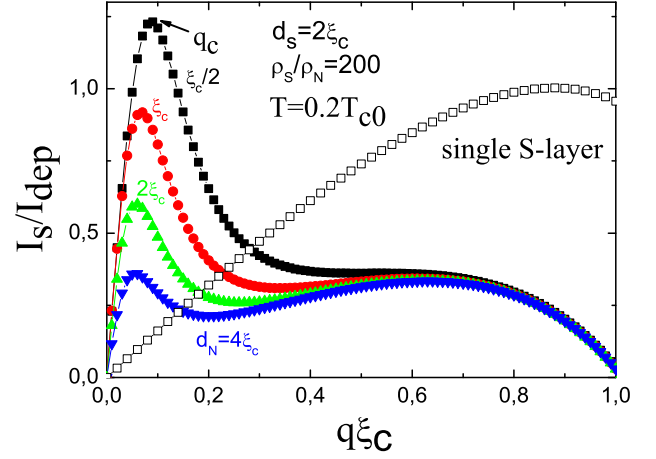


FIG. 2: Dependence of the superconducting current I_s (it is normalized to depairing current of single S-layer) flowing along the bilayer on q which is proportional to supervelocity $v_s \sim q$. Results are present for different thicknesses of N-layer $d_N/\xi_c = 1/2, 1, 2, 4$. Critical current corresponds to maximal possible value of I_s and for bilayers it is reached at $q\xi_c \sim 0.06 - 0.09$ for chosen parameters. In single S-layer maximum in dependence $I_s(q)$ (empty squares) is located at $q\xi_c \simeq 0.88$.

penetration depth $\Lambda^{-1} = \int dx/\lambda(x)^2$ (in a case of single superconducting layer with $\lambda(x) = const$, $\Lambda = \lambda^2/d_S$ - is the Pearl penetration depth [11]). Λ is normalized in units of $\Lambda_0 = \lambda(0)^2/d_S$, where $\lambda(0)$ is the London penetration depth of single S-layer at $T = 0$. Λ^{-1} describes the screening ability of bilayer and for relatively large ratio ρ_S/ρ_N and temperature not far below from T_c it could considerably exceeds Λ^{-1} of single S-layer (see Fig. 1(a)). This effect originates from relation $1/\lambda^2 \sim 1/\rho$ valid in the dirty limit and proximity induced superconductivity in N-layer (see inset in Fig. 1(a)). Besides one can see non-BCS (Bardeen-Cooper-Shreefer) like temperature dependence of Λ^{-1} which is consequence of the temperature dependence of superconducting order parameter $\Delta(d_S)$ near the SN interface (see inset in Fig. 1(b)) which controls the strength of induced superconductivity in N-layer. Value of $\Delta(d_S)$ depends not only on the temperature and ratio of resistivities but also on the thickness of N-layer. We consider the situation when $d_N < \xi_N(T_{c0})$ and even small variation of d_N or temperature leading to small change of ratio $d_N/\xi_N(T)$ strongly influences $\Delta(d_S)$ and Λ^{-1} due to large parameter $\rho_S/\rho_N \gg 1$ in the boundary condition for anomalous Green function F at SN interface: $dF/dx|_{d_S-0} = (\rho_S/\rho_N)dF/dx|_{d_S+0}$ and boundary condition $dF/dx|_{d_S+d_N} = 0$ at outer edge.

In Fig. 2 we present calculated dependence of superconducting current I_s flowing along the bilayer as a function of value $q = \nabla\phi - 2\pi A/\Phi_0$ (ϕ is a phase of superconducting order parameter, A is a vector potential, Φ_0 is the magnetic flux quantum) which is proportional to

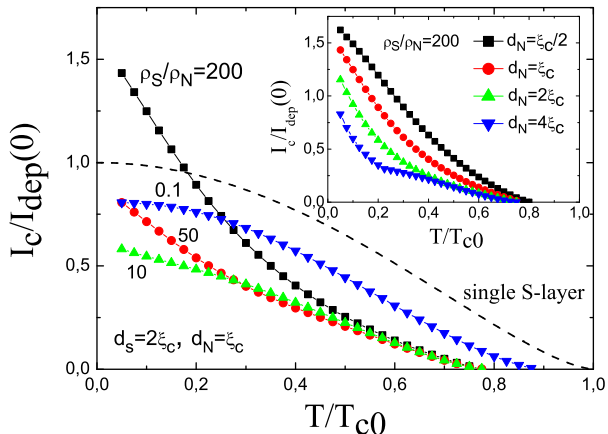


FIG. 3: Temperature dependence of the critical current of SN bilayer at different $\rho_S/\rho_N = 0.1, 10, 50, 200$ (dashed curve corresponds to temperature dependence of depairing current of single S-layer). In the inset we present temperature dependence of the critical current of SN bilayer at different thicknesses of N-layer $d_N/\xi_c = 1/2, 1, 2, 4$ and $d_S = 2\xi_c$. For bilayer with $d_N/\xi_c = 4$ dependence $I_c(T)$ has a kink at $T \simeq 0.22T_{c0}$ because of dominant contribution of N-layer in I_c at $T \lesssim 0.22T_{c0}$.

the superconducting velocity $v_s \sim q$ and those value does not vary across the bilayer (when parallel/perpendicular magnetic field $H_{\parallel,\perp} = 0$). In calculations we assume no vortices and uniform current distribution across the superconductor/bilayer. Note that this dependence may have two maxima in contrast with single superconducting film (see for example [12]). At $q < q_c$ (see Fig. 2) the major part of superconducting current flows via the normal layer (due to locally larger $1/\lambda^2$) while at $q > q_c$ proximity-induced superconductivity in N-layer is suppressed (λ^{-2} rapidly decreases with increasing $q > q_c$) and near the second maxima the major part of superconducting current flows via S-layer. For relatively small thickness of the N-layer the maximal (critical) superconducting current can exceed the depairing current of single superconducting film.

Temperature dependence of critical current of bilayer also is non-BCS like (see Fig. 3) and resembles temperature dependence of Λ^{-1} . Origin of this dependence comes from larger magnitude of proximity induced superconductivity in the N-layer when temperature decreases and corresponding increase of Λ^{-1} .

So far we present results for fixed thickness of S-layer $d_S = 2\xi_c$. We find that the nontrivial (non BCS like) temperature dependence $I_c(T)$ shifts to lower temperatures with increasing d_S - see Fig. 4(a) and in wide temperature interval ($0 \div T_c$) it exists only for relatively thin bilayers with $d_S \lesssim 2\xi_c$ (for realistic ratio $\rho_S/\rho_N \lesssim 200$). The reason is in increasing contribution of S-layer to the superconducting current when d_S increases while contribution of N-layer stays practically the same. Similar effect occurs with increasing d_N (at fixed d_S , T and

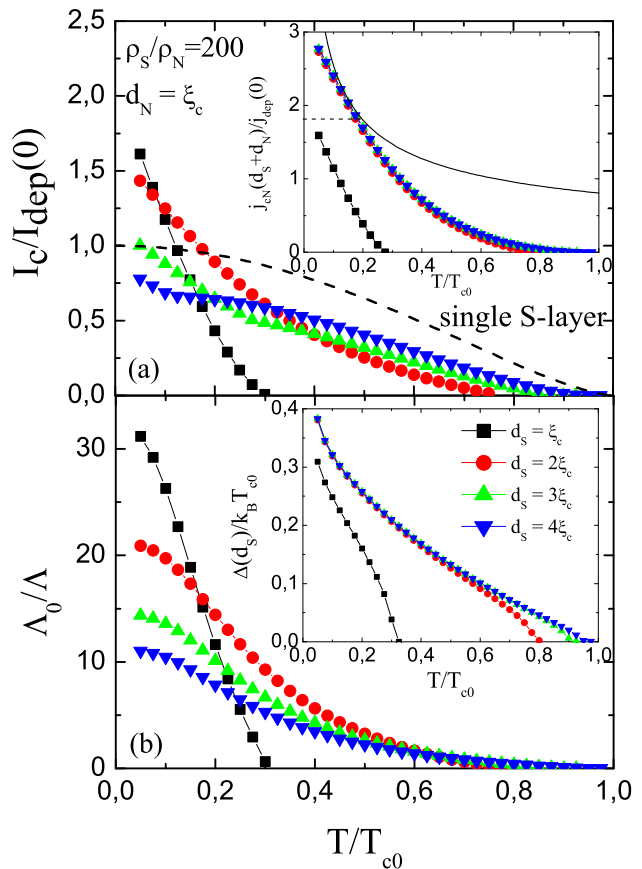


FIG. 4: Temperature dependence of I_c (a) and Λ^{-1} (b) of SN bilayer with different thicknesses of S-layer. With increasing d_S nontrivial temperature dependence of I_c shifts to lower temperatures where superconducting current mainly flows in N-layer. In inset to figure (a) we show temperature dependence of critical (maximal) superconducting current density in N-layer at outer boundary ($x = d_S + d_N$) and analytical expression for $j_{cN}(T)$ found in Ref. [9] (solid curve is Eq. (28) and dashed line is Eq. (30) from [9]). In inset to figure (b) we show temperature dependence of Δ at SN interface ($\Delta(d_S)$).

not very low temperatures) because of weaker induced superconductivity in N-layer. In inset to Fig. 4(a) we present calculated temperature dependent critical (maximal) superconducting current density in N-layer and its comparison with analytical results from Ref. [9] (solid and dashed curves - see Eq. (28) and (30), correspondingly, in [9]). Note qualitative similarity and quantitative difference.

In contrast, $\Lambda^{-1}(T)$ is non BCS like in wide temperature interval even for relatively large d_S - see Fig. 4(b). The reason for this is following. Critical current of bilayer is proportional to $q_c \Lambda^{-1}$, where q_c corresponds to maximum in dependence $I_s(q)$. In bilayer with $\rho_S/\rho_N \gg 1$ q_c is much smaller than in superconducting film (it roughly scales as $\sim \rho^{1/2}$). It results only to a little larger I_c in bilayer despite much larger Λ^{-1} in comparison with su-

perconducting film. As Λ_0/Λ decreases (for example with increasing d_S) the critical current is mainly determined by S-layer (except at very low T) while main contribution to Λ^{-1} still comes from N-layer when $q \ll q_c$.

Due to difference in critical supervelocities of S and N-layers value of critical current in 'positive' (I^+) and 'negative' (I^-) directions are different in parallel magnetic field ($I^\pm \perp H_{\parallel}$ - see inset in Fig. 5). Indeed, parallel magnetic field either increases $q = \nabla\phi - 2\pi A/\Phi_0$ in N-layer or decreases it depending on direction of the current (which is determined by direction of $\nabla\phi$). In the first case I_c rapidly decreases because q reaches q_c at smaller $\nabla\phi$ while in the second case I_c may even slightly increase at weak magnetic field (note that these fields weakly affect superconductivity in S-layer due to much larger value of q_c). Difference in I_c^\pm provides the diode effect (appearance of nonzero average voltage) in the regime with ac current (with zero time-averaged current). In Fig. 5 we show calculated dependence $I_c^\pm(H_{\parallel})$ for bilayer with following parameters: $d_N = d_S = 2\xi_c$, $\rho_S/\rho_N = 200$, $T = 0.2T_{c0}$. At large H_{\parallel} the superconductivity in N layer is suppressed and $I_c^- \simeq I_c^+$.

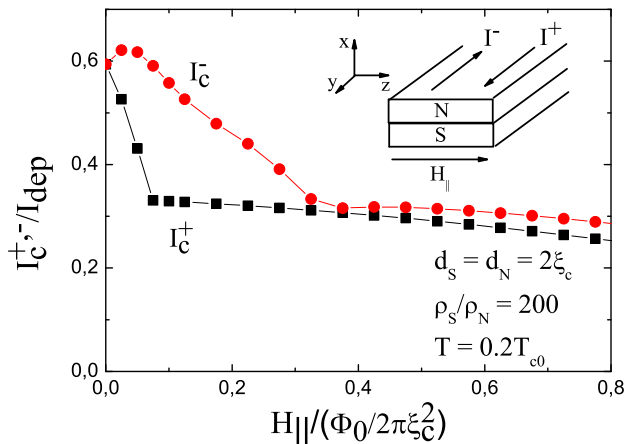


FIG. 5: Dependence of the critical current of SN bilayer on the parallel magnetic field. Currents flowing in opposite directions ('positive' and 'negative' - see inset) have different critical values when $H_{\parallel} \neq 0$ which is a consequence of different critical supervelocities in S and N layers.

Note that in symmetric SNS or NSN system the diode effect is absent. It is rather weak in SN bilayer with $\rho_S \lesssim \rho_N$ (comparable with one shown in Fig. 5 at large H_{\parallel}) because in this case the main part of superconducting current flows via S-layer. Therefore the presence of noticeable diode effect could be some kind of experimental verification of large/dominant contribution of N-layer in I_c at zero magnetic field.

III. EXPERIMENTAL RESULTS

To verify theoretical predictions we perform experiments on NbN/Al, NbN/Ag and MoN/Ag bilayers with $50 \lesssim \rho_S/\rho_N \lesssim 400$ and single NbN, MoN films. Using $T_{c0}(\text{NbN})=9$ K and $T_{c0}(\text{MoN})=7.5$ K we estimate $\xi_c = 6.5\text{nm}$ for NbN (we take $D_S = 0.5\text{cm}^2/\text{s}$ from [13]) and $\xi_c = 6.4\text{nm}$ for MoN (we take $D_S = 0.4\text{cm}^2/\text{s}$ from [14]). We have to mention, that critical temperature of our NbN and MoN films gradually decreases with decreasing their thickness when $d_S \lesssim 20\text{nm}$ (results for relatively thin MoN films are present in Ref. [14]). We relate this effect with presence of 'dead' nonsuperconducting layer with thickness $2 - 3\text{nm}$ at the interface with substrate. Proximity effect with this layer could provide decreasing T_c with decreasing d_S . Therefore we estimate the effective 'superconducting' thickness of our NbN and MoN in the range $11 - 13\text{nm}$ which is close to $2\xi_c$. In our experiment Λ^{-1} is measured using two coils technique [15] (via measurements of their mutual inductance M with sample between them) while I_c is extracted from current voltage characteristics of S and SN bridges. To study effect of the thickness of N-layer on superconducting properties of bilayer we change d_N by consequent ion etching (for experimental details see Appendix B).

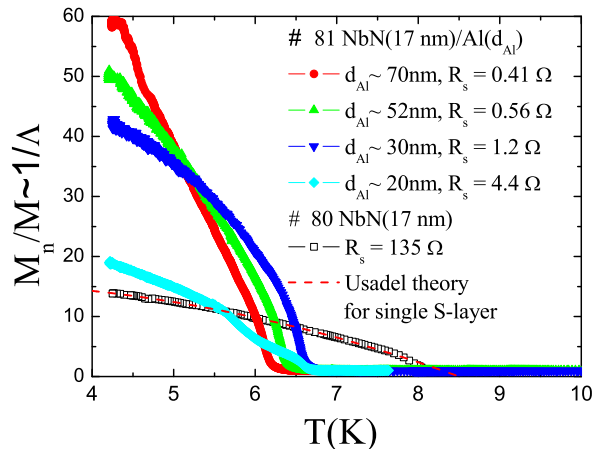


FIG. 6: Evolution of temperature dependence of Λ^{-1} of NbN/Al bilayer during etching and reference NbN film (measured mutual inductance M is normalized to its value in the normal state M_n just above T_c). Thickness of Al layer is estimated from measured room temperature resistance per square R_s (shown in the inset). Red dashed curve corresponds to dirty limit theoretical expectation for single superconducting layer: $\Lambda^{-1} \sim \tanh(\Delta(T)/2k_B T)$ [16].

In Fig. 6 we show evolution of experimental $\Lambda^{-1}(T)$ for NbN/Al bilayer during consequent etching of N-layer. One can see that the presence of normal layer considerably enhances screening abilities in comparison with the single superconducting film and effect becomes stronger at low temperatures. With decreasing d_N enhancement

becomes smaller at low temperatures, which qualitatively coincides with theoretical predictions (see Fig. 1(b)). Note that for thinnest Al layer shape of dependence $\Lambda^{-1}(T)$ is probably affected by nonuniformity of Al layer along the film (it appears during etching procedure and it is seen from our measurements of resistance per square R_s in different places of the sample). Not etched bilayer NbN/Al with similar d_{NbN} and $d_{\text{Al}} = 10\text{nm}$ shows much larger diamagnetic response (see Fig. 12 in Appendix C) and no signs of features in dependence $\Lambda^{-1}(T)$.

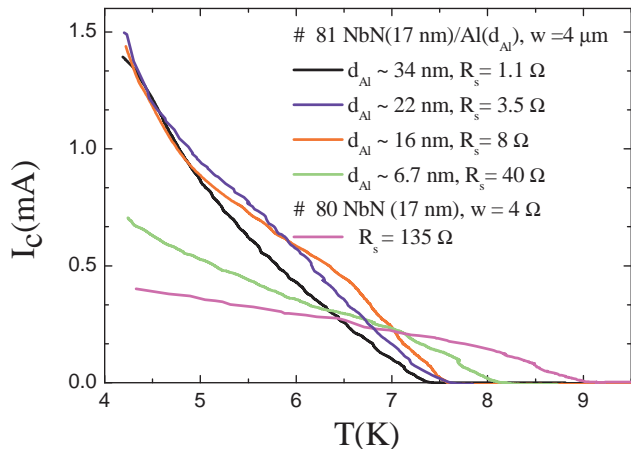


FIG. 7: Evolution of temperature dependence of critical current of NbN/Al bridge during etching procedure. For comparison we also show temperature dependence of critical current of NbN bridge. Thicknesses of Al layers are estimated from room temperature R_s (shown in the inset).

In Fig. 7 we show evolution of $I_c(T)$ of NbN/Al bridge with width $w = 4 \mu\text{m}$ during consequent etching (similar results are found for NbN/Ag bridge - see Fig. 13 in Appendix C). Because $\Lambda_0 = \lambda(0)^2/d_S \simeq 21 \mu\text{m}$ (for estimation we use $\lambda(0) = 600\text{nm}$ found from dirty limit expression $\lambda(0) = (\hbar\rho/\pi\mu_0 1.76k_B T_c)^{1/2}$ with $\rho = 300 \mu\Omega \cdot \text{cm}$ and $T_c = 9\text{K}$) and as it follows from Fig. 12 for NbN/Al bridge $\Lambda(4.2\text{K}) \simeq \Lambda_0/3 \simeq 7 \mu\text{m} > w$ we conclude that current flows uniformly across the bridge. One can see that even few nanometer Al layer modifies $I_c(T)$ in comparison with one for NbN bridge and makes it similar to the theoretical expectations. We also find that I_c of NbN/Al bridge with relatively large d_N exceeds critical current of NbN bridge in about 4 times at $T = 4.2\text{K}$. So large critical current enhancement we explain by low I_c of our NbN bridge, in comparison with its depairing current. Indeed, using theoretical expression following from the Usadel theory (see for example Eq. (30) in [17]), measured $R_s(T = 10\text{K}) = 150\Omega$, $T_{c0} = 9\text{K}$ for sample #80 and $D = 0.5\text{cm}^2/\text{s}$ we find $I_{dep}(4.2\text{K}) = 3.8\text{mA}$ which is 10 times larger than the measured critical current at $T = 4.2\text{K}$. The small critical current is probably connected with intrinsic inhomogeneities of our NbN films which allow vortex penetration and motion at supervelocity much lower than depairing supervelocity (which corresponds to maxima in dependence $I_s(q)$ for ideal S-layer - see Fig.

2). In bilayer value of critical supervelocity is mainly determined by N-layer (see maxima in dependencies $I_s(q)$ in Fig. 2) and it is order of magnitude smaller (for $\rho_S/\rho_N = 200$) than in ideal (defectless) superconducting film. Because Al-layer is rather homogenous (this fact follows from its relatively low resistivity and mean path length $\ell_N \sim d_N$) we expect that at $q < q_c$ vortices cannot penetrate our bilayer bridge. As a result the superconducting current of bilayer bridge approaches its maximal possible value (with main contribution from N-layer) which is about half of I_{dep} of NbN layer at this temperature (according to our calculations - see Fig. 3 for bilayers with close parameters).

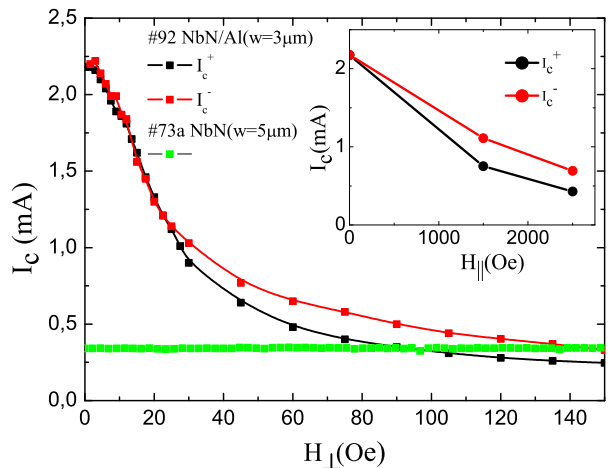


FIG. 8: Dependence of critical current (flowing in opposite directions) of NbN/Al ($d_{\text{NbN}} = 19\text{nm}$, $d_{\text{Al}} = 10\text{nm}$) and NbN ($d_{\text{NbN}} = 19\text{nm}$) bridges on perpendicular magnetic field H_{\perp} . For NbN bridge I_c does not depend on direction of the current and H_{\perp} . In the inset we show dependence I_c^{\pm} of the same NbN/Al bridge on the parallel magnetic field.

Support for such an explanation comes from dependence of I_c on perpendicular magnetic field H_{\perp} present in Fig. 8. In NbN bridge I_c does not depend on H_{\perp} at weak magnetic fields which confirms the idea that critical current is determined by bulk pinning of the vortices with pinning current density $j_p \ll j_{dep}$. Contrary, in NbN/Al bridge the shape of dependence $I_c(H)$ says in favor of edge barrier controlled vortex penetration and motion [18]. From dependence $I_c(H)$ one can estimate value of q_c in N-layer and compare it with corresponding value of single S-layer. From the edge barrier theory it follows that at $H^* \simeq q_c \Phi_0 / 2\pi w$ critical current drops in 2 times in comparison with $I_c(H = 0)$. For $3 \mu\text{m}$ bridge $H^* \simeq 25\text{Oe}$ (see Fig. 8) and $q_c \xi_c \simeq 0.15$ which is much smaller than $q_c \xi_c \simeq 0.68$ for single S layer at $T = 0.5T_{c0}$.

Our measurements in parallel magnetic field revealed the diode effect - value of the critical current depends on direction of its flow (see inset in Fig. 8). In the experiment difference $I_c^+ - I_c^-$ is smaller than the theory predicts (compare Fig. 5 and inset in Fig. 8). We be-

lieve that it is connected with the presence of perpendicular component of the magnetic field which strongly suppresses proximity induced superconductivity in N-layer and I_c^\pm . Note, that in the experiment $I_c^+ \neq I_c^-$ in the perpendicular magnetic field too (most probably it is connected with different quality of edges of the bridge [19]) but relative difference is smaller than in the parallel magnetic field.

IV. DISCUSSION

We present results on superconducting properties of thin dirty SN bilayer with thickness of S layer d_S about several ξ_c , thickness of N layer $d_N \ll \xi_N(T_{c0})$ and large ratio of residual resistivities $\rho_S/\rho_N \gg 1$. We show that such a bilayer has unique superconducting properties. First of all the screening ability of the bilayer is determined mainly by the proximity induced superconductivity in the normal layer, where locally the London penetration depth λ is smaller. Secondly, at some conditions, the presence of normal layer may considerably increase the critical current (the effect is not connected with enhanced vortex pinning) because the largest part of superconducting current flows via the normal layer where superconducting current density $j_s \sim 1/\lambda^2$. Besides the temperature dependence of critical current and effective magnetic field penetration depth have unusual, non-BCS like temperature dependence. We argue that these properties are consequences of small thickness of N-layer and large ratio of resistivities $\rho_S/\rho_N \gg 1$.

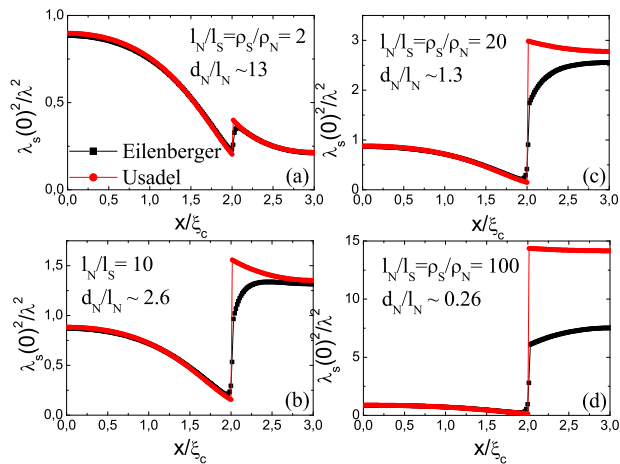


FIG. 9: Dependence of local $1/\lambda^2$ on the coordinate across the bilayer ($d_S = 2\xi_c$, $d_N = \xi_c$, $T = 0.2T_{c0}$) calculated in Usadel and Eilenberger (see for example Eq. (1) in [23]) models for different ratios of resistivities (mean path lengths).

We believe that our results could be used as an alternative explanation for the several times enhancement of I_c found in NbN/CuNi bilayers in comparison with single NbN film [20, 21]. The thickness of NbN layer

was 8 nm, while the thickness of CuNi layer varied from 3 up to 6 nm. It is known that residual resistivity of CuNi strongly depends on Ni concentration and varies in the range $\rho_{\text{CuNi}} \simeq 2 - 49 \mu\Omega \cdot \text{cm}$ [22] and, hence, potentially the ratio $\rho_{\text{NbN}}/\rho_{\text{CuNi}}$ could reach 100 (with $\rho_{\text{NbN}} = 200 \mu\Omega \cdot \text{cm}$). Unfortunately due to absence of dependence $I_c(T)$ and actual values of resistivity of used CuNi and NbN layers we cannot make a solid statement about the role of proximity effect in that experiments.

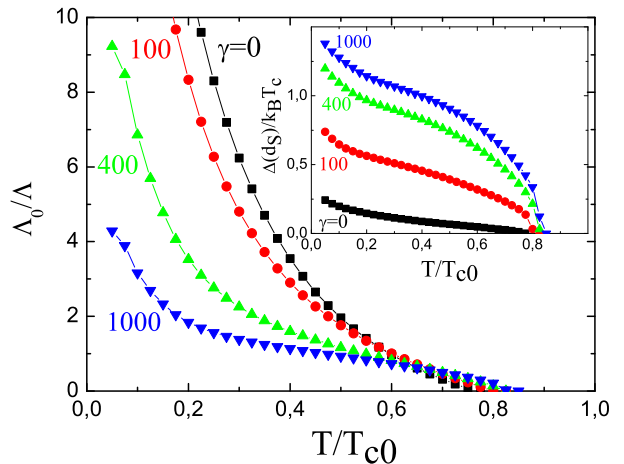


FIG. 10: Temperature dependence of Λ^{-1} for bilayer with $d_S = d_N = 2\xi_c$, $\rho_S/\rho_N = 200$ and finite barrier between S and N layers (strength of the barrier is governed by parameter γ - see Eq. A6). In the inset we present temperature dependence of $\Delta(d_S)$ at different γ . Result are obtained using Usadel model.

Our experimental findings confirm main predictions of the theory but there is quantitative discrepancy between theory and experiment. The main difference is that in the experiment effect of N-layer is stronger than Usadel model gives. First of all T_c of bilayer changes with change of d_N stronger and Λ^{-1} is larger in the experiment than in the theory (compare Fig. 1(a) with Fig. 6 and Fig. 11 in Appendix C). Secondly, there is a difference in the predicted shape of dependence $\Lambda^{-1}(T)$ and experimental one for relatively small d_N . And finally, critical current of the bilayer is larger in the experiment. For example for sample #92 ($d_{\text{NbN}} = 19 \text{ nm}$, $d_{\text{Al}} = 10 \text{ nm}$, $w = 3 \mu\text{m}$ - see Fig. 8) experimental critical current of bilayer approaches I_{dep} of host superconductor already at $T = 4.2 \text{ K} = 0.47 T_{c0}$ while theory predicts only $I_c = 0.29 - 0.31 I_{dep}$ depending on the chosen ratio $\rho_S/\rho_N = 50 - 200$ (in calculations we use $d_S = 2\xi_c$ and $d_N = 1.5\xi_c$).

These quantitative discrepancies are not related to the usage of Usadel theory in N-layer where mean path length $\ell_N \sim d_N$ or finite transparency of SN-interface (both of them lead to decreasing of Λ^{-1} - see Figs. 9 and 10). Even if one takes into account dependence of ρ_N on d_N it provides only a little better quantitative fit to the experiment. The origin of the difference could be related

with very short mean path length ℓ_S in NbN and MoN materials which is in the range of 1\AA if one uses relation $D_S = v_F \ell_S / 3$ with typical value of Fermi velocity $v_F = 2 \cdot 10^8 \text{cm}^2/\text{s}$. It questions about boundary conditions for quasiclassical Green functions at SN interface between highly disordered superconductor and relatively clean metal and how it affects both direct and inverse proximity effects in N and S layers.

Due to strong dependence of I_c on temperature such a SN bilayer has unclear perspectives from point of view applications where one needs large critical current. Besides effect of current enhancement could be noticeable only in relatively thin structures and when host superconductor has critical current much smaller than depairing current. From another side steep temperature dependence of I_c and Λ^{-1} could be utilized in different kinds of superconducting detectors of electromagnetic radiation [24, 25], particles [26] or dark matter [27] based on temperature dependent $I_c(T)$ and/or $\Lambda^{-1}(T)$. For example in superconducting single photon detector (SSPD) absorbed photon or particle locally heats by δT the superconducting strip biased below its critical current $I < I_c(T)$ and the superconductor transits to the resistive state when $I > I_c(T + \delta T)$ [24]. In the kinetic inductance detector (KID) such a heating leads to change of kinetic inductance $L \sim \Lambda^{-1}(T)$ and resonance frequency of corresponding inductance-capacity circuit [25]. It is clear that the steeper the temperature dependence of I_c , Λ^{-1} the larger will be their change at fixed δT (it is determined by energy of absorbed particle or photon) and sensitivity of detector should subsequently increase.

Another advantage of SN bilayer in comparison with highly disordered superconductors is connected with high uniformity of N-layer. Our results show that proximity induced superconductivity in N-layer is weakly sensitive to local inhomogeneities of host superconductor (it follows from our measurements of $I_c(H)$ for SN bilayer - see Fig. 8) and critical current of bilayer approaches to its maximal possible value. Note, that in superconductors with large ρ the value of critical current is dictated by the weakest place in the sample and usually it is smaller than the depairing current in two or more times [28].

Acknowledgments

The work is supported by the Russian Scientific Foundation, grant No. 15-12-10020 (A.V.P., A.M.K.) and grant No. 17-72-30036 (D.Yu.V.). E.E.P., S.S.U., M. Yu. L. and A.I.E. acknowledge support from Russian Foundation for Basic Research, grants No 15-42-02365 and No 15-42-02469. The authors also thank N.V. Rogozhkina and A.N. Kovtun for the help with the samples fabrication. The facilities of the Common Research Center Physics and Technology of Micro- and Nanostructures of Institute for Physics of Microstructures of RAS were used.

Appendix A: Model

To calculate superconducting properties of SN bilayer we use Usadel equation for anomalous $F = \sin \Theta$ and normal $G = \cos \Theta$ Green functions

$$\hbar D \frac{\partial^2 \Theta}{\partial x^2} - \left(2\hbar\omega_n + \frac{D}{\hbar} q^2 \cos \Theta \right) \sin \Theta + 2\Delta \cos \Theta = 0, \quad (\text{A1})$$

where D is a diffusion coefficient ($D = D_S$ in superconducting layer and $D = D_N$ in the normal one), $\omega_n = \pi T(2n + 1)$ is a Matsubara frequency, $q = \nabla\varphi - (2\pi/\Phi_0)A(x)$ (φ is a phase of the order parameter, A is a vector potential) takes into account nonzero velocity of superconducting condensate $v_s \sim q$ in direction parallel to layers (y direction in our case), $\Delta(x)$ is a magnitude of superconducting order parameter which has to be found in the superconducting layer with help of self-consistency equation

$$\Delta \ln \left(\frac{T}{T_{c0}} \right) + 2\pi k_B T \sum_{\omega_n \geq 0} \left(\frac{\Delta}{\hbar\omega_n} - \sin \Theta_s \right) = 0 \quad (\text{A2})$$

and we assume that in the normal layer $\Delta = 0$ because of zero BCS coupling constant. T_{c0} in Eq.(A2) is the critical temperature of superconductor with no N-layer.

We consider thin bilayer with thickness of superconducting layer $d_S \ll \lambda$ (λ is the London penetration depth) and thickness of normal layer d_N less than characteristic penetration depth of magnetic field in N layer. Therefore we may neglect corrections to $A(x)$ which comes from screening effect and choose following form for $A(x) = H_{\parallel} x$ (H_{\parallel} is a parallel magnetic field).

The inverse effective magnetic field penetration depth by definition is

$$\Lambda^{-1} = \frac{16\pi^2}{\hbar c^2} \int_0^{d_s+d_n} \frac{1}{\rho} \sum_{\omega_n \geq 0} \sin^2 \Theta dx \quad (\text{A3})$$

with $\rho = \rho_S$ in S layer and $\rho = \rho_N$ in N layer. In the absence of normal layer $\Lambda = \lambda^2/d_S$ - so called Pearl penetration depth.

To find the sheet critical current (critical current per unit of width of the bilayer) we use the following expression for sheet superconducting current

$$J = \int_0^{d_s+d_n} \frac{2\pi k_B T}{e\hbar\rho} q \sum_{\omega_n \geq 0} \sin^2 \Theta dx \quad (\text{A4})$$

The sheet critical current is defined as maximal sheet superconducting current. For superconducting film without N-layer $J_c = j_{dep} d_s$, where j_{dep} is the depairing current.

At SN interface ($x = d_S$) we use Kupriyanov-Lukichev boundary conditions [29]

$$D_s \frac{d\Theta}{dx} \Big|_{x=d_s-0} = D_n \frac{d\Theta}{dx} \Big|_{x=d_s+0} \quad (\text{A5})$$

$$\gamma \xi_c \left. \frac{d\Theta}{dx} \right|_{x=d_s+0} = \sin(\Theta(d_s+0) - \Theta(d_s-0)) \quad (\text{A6})$$

and boundary condition with vacuum at $x=0, d_s+d_n$: $d\Theta/dx=0$. Eq. (A6) leads to jump of Θ on SN boundary in presence of the barrier, which is controlled by parameter $\gamma = R_{SN}A_{SN}/(\sigma_N\xi_c)$ (R_{SN} is the resistance of SN interface, A_{SN} is its area and $\xi_c = \sqrt{\hbar D_S/k_B T_{c0}}$). Usually we choose $\gamma=0$ which leads to continuity of Θ : $\Theta(d_S+0) = \Theta(d_S-0)$.

Equations (A1,A2) are solved numerically by using iteration procedure. For initial distribution $\Delta(x) = \text{const}$ we solve Eq. (A1) for Matsubara frequencies ranging from $n=0$ up to $n=100$. In numerical procedure we use Newton method combined with tridiagonal matrix algorithm. Found solution $\Theta(x)$ is inserted to Eq. (A2) to find $\Delta(x)$ and than iterations repeat until the relative change in $\Delta(x)$ between two iterations does not exceed 10^{-8} . Length is normalized in units of ξ_c , energy is in units of $k_B T_{c0}$, current is in units of depairing current of single S-layer with the thickness d_S , magnetic field is in units of $H_0 = \Phi_0/2\pi\xi_c^2$ and effective magnetic field penetration depth is in units of $\Lambda_0 = \lambda^2(T=0)/d_S$. Usual step grid in S and N layers is $\delta x = 0.02\xi_c$.

To decrease the number of free parameters we suggest that the density of states in S and N layers are the same and ratio of resistivities is equal to inverse ratio of diffusion constants or mean path lengths $\rho_S/\rho_N = D_N/D_S = \ell_N/\ell_S$.

Appendix B: Experimental details

The bilayers NbN/Ag and NbN/Al were prepared on Al_2O_3 $10 \times 10 \text{ mm}^2$ substrates in a magnetron vacuum machine (Alcatel SCM-600) with a load-lock chamber. The thin films were fabricated in a single deposition run at the substrates at ambient temperatures. In total three targets were used: pure niobium (99.9%) as a superconducting material, Al ((99.99%) and Ag (99.99%) as the normal metals. The design of the deposition machine allows growth of the entire structure in one cycle without disrupting the vacuum. This results in high-quality structures with clean interfaces and strong proximity effect. NbN films were deposited by reactive dc-magnetron sputtering in the Ar (99.999%) and N₂ (99.999%) gases mixed at the total pressure of 7×10^{-3} mbar with a residual pressure in the chamber of about 1.5×10^{-7} mbar. The deposition rate of the NbN layers was 1.3 nm/s. The Ag and Al films were deposited by rf-magnetron sputtering in the Ar at the pressure of 2×10^{-2} mbar. The deposition rates of the Ag and Al layers were from 1 to 3 nm/s.

MoN/Ag was fabricated by DC-magnetron sputtering on HV system AJA ATC-2200 at room temperature. All samples were fabricated on a silicon substrate (KDB-10) in one vacuum cycle and covered by Si (10 nm) to protect

of oxidation a top layer. MoN film was deposited from metallic Mo target in N₂ atmosphere, see [14]. The base vacuum in the main chamber was about 2×10^{-8} mbar. The working pressure was maintained at a level of 2.6×10^{-8} mbar. The rate of deposition of layers was about 3-5 nm/min.

Measurements of Λ^{-1} were performed by using standard two-coil measurement technique of mutual inductance (see for example Ref. [15]). The diameter of coils (2 mm) and their height (4 mm) is smaller than the typical lateral size of measured film (10×10 or 7×7 mm), separation between coils is ~ 1 mm, while thickness of the bilayer $d_s + d_n < 100$ nm is smaller than London penetration depth. At these parameters mutual inductance $M \sim \Lambda$ [15] except temperatures close to T_c where Λ diverges.

The bridges made of bilayer films were fabricated by standard lift-off lithography. Because of low substrate temperature we were able to deposit the bilayers on the photoresist without its apparent degradation. Widths of the bridges range from 3 up to 5 microns, while their length is fixed to 10 microns. Due to low thickness of studied bilayer bridges ($d_{\text{NbN}} = 12 - 19 \text{ nm}$, $d_{\text{MoN}} = 19 \text{ nm}$, $d_{\text{Al}} = 2 - 25 \text{ nm}$, $d_{\text{Ag}} = 2 - 30 \text{ nm}$) current density distribution across the sample is expected to be uniform because $w < \Lambda$. Transport measurements were performed by four-probe method. During measurements we change the current from large negative up to large positive values and in this way we were able to find both the critical current I_c (at this current bridge switches from the superconducting state to the resistive one) and re-trapping current I_r (when the bridge switches back from the resistive to the superconducting state).

Resistivity of the samples was measured either using van Der Pauw method and/or transport measurements. In this way we find $\rho_{\text{NbN}} = 260 - 380 \mu\Omega \cdot \text{cm}$ depending on the sample and $\rho_{\text{MoN}} = 200 \mu\Omega \cdot \text{cm}$ at $T = 10 \text{ K}$. For both materials room temperature ρ is smaller than at $T = 10 \text{ K}$ which is common feature of highly disordered metallic films. Our thickest Al film ($d_{\text{Al}} = 70 \text{ nm}$) has $\rho_{\text{Al}} = 2.9 \mu\Omega \cdot \text{cm}$ while 90 nm thick Ag film has $\rho_{\text{Ag}} = 1.5 \mu\Omega \cdot \text{cm}$ (both at room temperature) which are close to literature data [30]. Residual resistance for these and thinner films is 1-4 times smaller and gradually increases with decreasing d_N [30] which gives us $\rho_S/\rho_N \lesssim 400$ depending on the thickness of the normal layer and the pair of S,N materials.

To study effect of the thickness of normal layer on superconducting properties of bilayer we make chips with side $10 \text{ mm} \times 10 \text{ mm}$. The central part of chips with size $6 \text{ mm} \times 6 \text{ mm}$ is used for measurements of mutual inductance, while on the edge of the chip we fabricate bridges. The thickness of Al and Ag layers is changed by gradual ion etching. The ion etching of Al and Ag layers was performed in a Plasmalab 80 plus (Oxford Instruments) equipped with capacitive (HF) and inductive (ICP) plasma sources. The etching process was performed in Ar at the pressure of 5 mbar, HF power

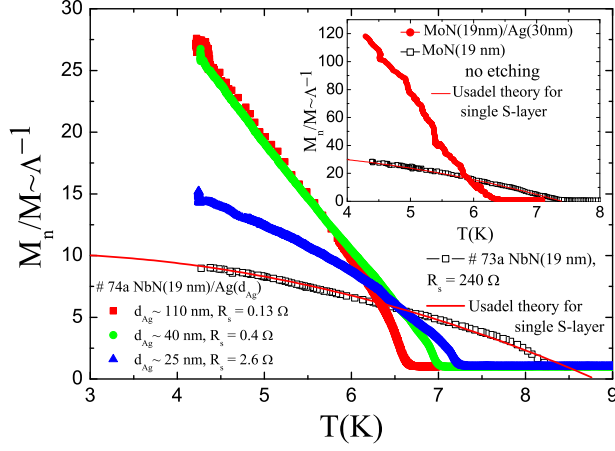


FIG. 11: Evolution of temperature dependence of Λ^{-1} of NbN/Ag bilayer after consequent etching and reference NbN film (mutual inductance is normalized to its value in the normal state just above T_c). In the inset we present $\Lambda^{-1}(T)$ for MoN/Ag bilayer ($R_s = 0.73\Omega$ at room temperature) with $d_{\text{MoN}} = 19\text{nm}$, $d_{\text{Ag}} = 30\text{nm}$ and single MoN layer ($R_s = 120\Omega$) with $d_{\text{MoN}} = 19\text{nm}$.

100 W and ICP power 400 W. The Ag etching rate was 30nm/min and Al etching rate 1 nm/min.

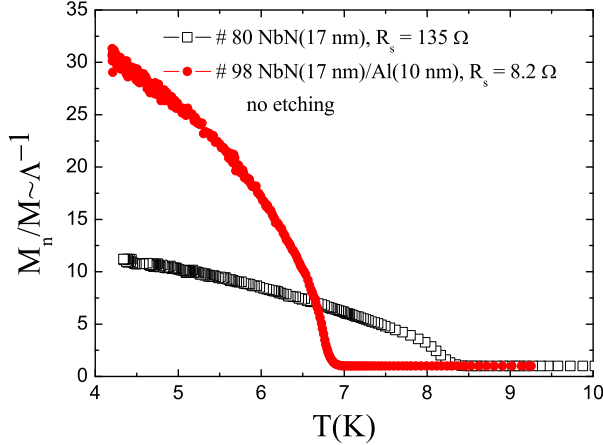


FIG. 12: Temperature dependence of Λ^{-1} of NbN/Al bilayer (sample #98, $d_{\text{NbN}} = 17\text{nm}$, $d_{\text{Al}} \simeq 10\text{nm}$, room temperature $R_s = 8.2\Omega$) and NbN film (sample #80, $d_{\text{NbN}} = 17\text{nm}$, room temperature $R_s = 135\Omega$).

We also did special experiment and find dependence of resistance per square R_s of normal layer on its thickness at room temperature during etching procedure combined with simultaneous measurement of the resistance of the etched sample. We use these results to estimate thick-

nesses of the Al and Ag layers in bilayer by measuring their room temperature R_s .

Appendix C: Experimental results for NbN/Ag and MoN/Ag bilayers

In Fig. 11 we present experimental $\Lambda^{-1}(T)$ for NbN/Ag bilayer after two consequent etching of N-layer. In the inset to Fig. 11 we show results for MoN/Ag bilayer and in Fig. 12 for NbN/Al bilayer without etching. Qualitatively these results coincide with ones for NbN/Al bilayers and theoretical calculations in the Usadel model. Quantitatively in the experiment Λ^{-1} is larger than the theory predicts.

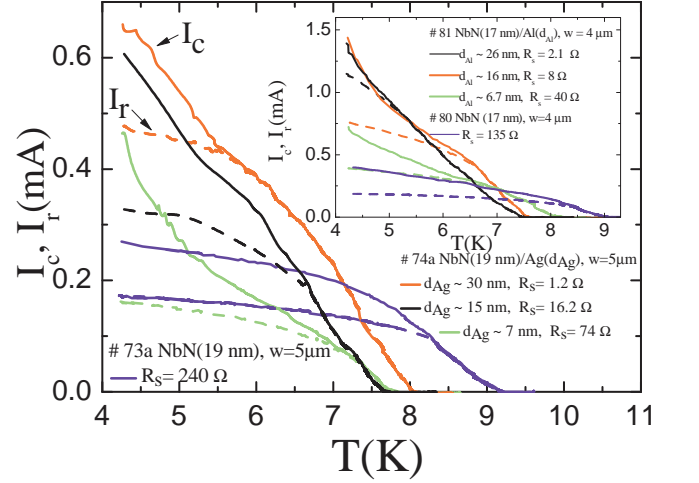


FIG. 13: Temperature dependence of critical (solid curves) and retrapping (dashed curves) currents of NbN/Ag and NbN/Al bridges (see inset) with different thicknesses of Al and Ag layers. In the same figures we show $I_c(T)$ and $I_r(T)$ of reference NbN bridges.

In Fig. 13 we show temperature dependence of critical I_c and retrapping I_r currents of NbN/Ag bridge with width $w = 5\mu\text{m}$ during consequent etching (in the inset results for NbN/Al bridge with $w = 4\mu\text{m}$ are present). The presence on the normal layer not only considerably increases the critical current and changes its temperature dependence in comparison with superconducting bridge but it also wipes out the hysteresis of current-voltage characteristics (making $I_r = I_c$) for bilayers with relatively large d_N . The last effect was observed earlier for shunted MoGe superconducting bridge with low shunt resistance [31]. The dependence $I_c(T)$ looks more 'noisy' for NbN/Ag bridges than for NbN/Al ones. The origin of the 'noise' comes from stochastic nature of switching to the resistive state [31] and it is clear seen in our experiment via repeated measurements of current-voltage characteristics at fixed temperature.

[1] Y. Oda and H. Nagano, *Meissner effect in Cu of thick Cu clad Nb*, Solid State Commun. **35**, 631 (1980).

[2] Th. Bergmann, K. H. Kuhl, B. Schröder, M. Jutzler, and

- F. Pobell, *Proximity-Effect-Induced Superconductivity at Millikelvin Temperatures*, J. Low Temp. Phys. **66**, 209 (1987).
- [3] A. C. Mota, P. Visani, and A. Pollini, *Magnetic Properties of Proximity-Induced Superconducting Copper and Silver*, **76**, 465 (1989).
- [4] A.D. Zaikin, *Meissner effect in superconductor-normal metal proximity sandwiches*, Solid State Commun. **41**, 533 (1982).
- [5] M. S. Pambianchi, J. Mao, and S. M. Anlage, *Magnetic screening in proximity-coupled superconductor/normal-metal bilayers* Phys. Rev. B **50**, 13659 (1994).
- [6] W. Belzig, C. Bruder, and G. Schön, *Diamagnetic response of normal-metal/superconductor double layers*, Phys. Rev. B **53**, 5727 (1996).
- [7] Alban L. Fauchère and G. Blatter, *Magnetic breakdown in a normal-metal/superconductor proximity sandwich*, Phys. Rev. B **56**, 14102 (1997).
- [8] A.V. Galaktionov and A. D. Zaikin, *Proximity-induced screening and its magnetic breakdown in mesoscopic hybrid structures*, Phys. Rev. B **67**, 184518 (2003).
- [9] L. G. Aslamazov, A. A. D'yachkov, and S. V. Lempitskii, *Properties of an anisotropic disordered system of superconductors in a normal metal*, Sov. Phys. JETP **64**, 1051 (1986).
- [10] S. V. Lempitskii, *Properties of an anisotropic system composed of a superconductor and a normal phase* Physica C **167** 168 (1990).
- [11] J. Pearl, *Current distribution in superconducting films 'carrying quantized fluxoids'*, Appl. Phys. Lett. **5** 65 (1964).
- [12] J. Romijn, T. M. Klapwijk, M. J. Renne, and J. E. Mooij, *Critical pair-breaking current in superconducting aluminum strips far below T* , Phys. Rev. B **26**, 3648 (1982).
- [13] A. Engel, A. Aeschbacher, K. Inderbitzin, A. Schilling, K. Ilin, M. Hofherr, M. Siegel, A. Semenov, and H.-W. Hubers, *Tantalum nitride superconducting single-photon detectors with low cut-off energy*, Appl. Phys. Lett. **100**, 062601 (2012).
- [14] Yu. Korneeva, I. Florya, S. Vdovichev, M. Moshkova, N. Simonov, N. Kaurova, A. Korneev, and G. Goltsman *Comparison of Hot Spot Formation in NbN and MoN Thin Superconducting Films After Photon Absorption*, IEEE Trans. on Appl. Supercond., **27**, 2201504 (2017).
- [15] J. H. Claassen, J. M. Byers and S. Adrian *Optimizing the two-coil mutual inductance measurement of the superconducting penetration depth in thin films* J. Appl. Phys. **82**, 3028 (1997).
- [16] M. Tinkham, *Introduction to superconductivity*, (McGraw-Hill, NY, 1996).
- [17] John R. Clem and V. G. Kogan, *Kinetic impedance and depairing in thin and narrow superconducting films*, Phys. Rev. B **86**, 174521, (2012).
- [18] B. L. T. Plourde, D. J. Van Harlingen, D. Y. Vodolazov, R. Besseling, M. B. S. Hesselberth, P. H. Kes, *Influence of edge barriers on vortex dynamics in thin weak-pinning superconducting strips*, Phys. Rev. B **64**, 014503 (2001).
- [19] D. Y. Vodolazov, F. M. Peeters, *Superconducting rectifier based on the asymmetric surface barrier effect*, Phys. Rev. B **72**, 172508 (2005).
- [20] N. Marrocco, G. P. Pepe, A. Capretti, L. Parlato, V. Pagliarulo, G. Peluso, A. Barone, R. Cristiano, M. Ejrnaes, A. Casaburi, N. Kashiwazaki, T. Taino, H. Myoren, and Roman Sobolewski, *Strong critical current density enhancement in NiCu/NbN superconducting nanostripes for optical detection*, Appl. Phys. Lett. **97**, 092504 (2010).
- [21] U. Nasti, L. Parlato, M. Ejrnaes, R. Cristiano, T. Taino, H. Myoren, Roman Sobolewski, and G. Pepe, *Thermal fluctuations in superconductor/ferromagnet nanostripes*, Phys. Rev. B **92**, 014501 (2015).
- [22] C. Y. Ho, M. W. Ackerman, K. Y. Wu, T. N. Havill, R. H. Bogaard, R. A. Matula, S. G. Oh, and H. M. James *Electrical resistivity of ten selected binary alloy systems*, Journal of Physical and Chemical Reference Data **12**, 183 (1983).
- [23] W. Belzig, C. Bruder and A. L. Fauchere, *Diamagnetic response of a normal-metal/superconductor proximity system at arbitrary impurity concentration*, Phys. Rev. B **58**, 14531 (1998).
- [24] C. M. Natarajan, M. G. Tanner and R. H. Hadfield, *Superconducting nanowire single-photon detectors: physics and applications*, Supercond. Sci. Technol. **25**, 063001 (2012).
- [25] P. K. Day, H. G. LeDuc, B. A. Mazin, A. Vayonakis, J. Zmuidzinas, *A broadband superconducting detector suitable for use in large arrays*, Nature **425**, 817 (2003).
- [26] H. Shishido, H. Yamaguchi, Y. Miki, S. Miyajima, K. Oikawa, M. Harada, M. Hidaka, T. Oku, M. Arai, A. Fujimaki and T. Ishida, *Neutron detection using the superconducting Nb-based current-biased kinetic inductance detector*, Supercond. Sci. Technol. **30**, 094003 (2017).
- [27] Y. Hochberg, Y. Zhao, and K. M. Zurek, *Superconducting Detectors for Superlight Dark Matter*, Phys. Rev. Lett. **116**, 011301 (2016).
- [28] R. Lusche, A. Semenov, K. Ilin, M. Siegel, Y. Korneeva, A. Trifonov, A. Korneev, G. Goltsman, D. Vodolazov, and H.-W. Hubers, *Effect of the wire width on the intrinsic detection efficiency of superconducting-nanowire single-photon detectors*, J. of Appl. Phys. **116**, 043906 (2014).
- [29] M. Yu. Kupriyanov and V. F. Lukichev, *Influence of boundary transparency on the critical current of "dirty" SS'S structures*, Sov. Phys. JETP **67**, 1163 (1988).
- [30] J. W. C. De Vries, *Temperature and thickness dependence of the resistivity of thin polycrystalline aluminium, cobalt, nickel, palladium, silver and gold films*, Thin Solid Films **167**, 25 (1988).
- [31] M. W. Brenner, D. Roy, N. Shah, and A. Bezryadin, *Dynamics of superconducting nanowires shunted with an external resistor*, Phys. Rev. B **85**, 224507 (2012).